Micromagnetism and variable-range hopping conductivity in $Fe_{1-x}In_xCr_2S_4$

Zhe Qu, Zhaorong Yang, Shun Tan, and Yuheng Zhang*
Structure Research Laboratory, University of Science and Technology of China, Hefei 230026, People's Republic of China
(Received 22 November 2004; revised manuscript received 24 March 2005; published 31 May 2005)

In $FeCr_2S_4$ with colossal magnetoresisitance effect, there are neither heterovalence nor Jahn-Teller (JT) distortion, hence double-exchange and JT effect can be excluded. It is proved that magnetic polarons hopping is responsible for the transport behavior in $FeCr_2S_4$ above T_c. Here, we report that in the system $Fe_{1-x}In_xCr_2S_4$, there is the magnetic fluctuation in the high temperature region. The transport properties in the high temperature region are dominated by variable-range hopping process. This can be ascribed to the magnetic random potential induced by the magnetic fluctuation. By studying the electron-spin-resonance (ESR) spectra of the single crystal with different angle, we successfully explain the intricate ESR behaviors that only a single line with $g<2$ is observed below T_c and splitting peaks are exhibited when $T<T_s$ in polycrystalline samples.

DOI: 10.1103/PhysRevB.71.184430 PACS number(s): 64.75.+g, 76.50.+g, 72.15.Rn

I. INTRODUCTION

The discovery of colossal magnetoresistance (CMR) effect in doped manganites with perovskite structure has fascinated considerable interest for its possible application and scientific significance in the past decade.[1–4] The essential physical mechanism in this system is believed to be double-exchange (DE) and Jahn-Teller (JT) effect.[5,6]

However, chalcogenide spinels, such as $FeCr_2S_4$, are another kind of CMR material. There are neither heterovalence nor JT effect.[7,8] The conductivity in $FeCr_2S_4$ was believed to originate from an Fe^{2+} narrow band.[9] Its magnetoresistance mechanism is initially speculated to arise from scattering between carriers and critical fluctuation.[10] In addition, the magnetism of $FeCr_2S_4$ is ferrimagnetic, both Fe sublattice and Cr sublattice are ferromagnetic, while the arrangement between two sublattices is antiferromagnetic. This kind of magnetic arrangement will inevitably influence the conductive properties. Previous works prove that magnetic polaron hopping is responsible for the transport properties at temperature above T_c.[11]

In order to probe the mysteries of great difference of the conductive mechanism between manganites and spinels, the transport mechanism in chalcogenide spinels need further to be investigated. We design a series of In doped samples $Fe_{1-x}In_xCr_2S_4$ ($x=0, 0.05, 0.10$), through which the influence of *A* site doping on magnetic and transport behavior is studied. Our results indicate that in all doped samples, the In ion occupies the Fe site in the form of In^{2+}. The magnetic fluctuation is observed above T_c in doped samples. It is found that the transport mechanism is the variable-range hopping in the high temperature region. This is attributed to the magnetic random potential which is induced by the magnetic fluctuation. In addition, by studying the ESR lines of the single crystal with different angle, we understand the intricate ESR behavior in polycrystalline samples properly.

II. EXPERIMENTAL DETAILS

Polycrystalline samples of $Fe_{1-x}In_xCr_2S_4$ ($x=0,0.05,0.10$) were prepared by conventional solid-state method.[7] High-purity powders of iron (99.9%), indium (99.9%), chromium (99.9%), and sulphur (99.999%) were mixed uniformly in a 2 g batch according to the stoichiometric ratio and sealed into evacuated quartz tubes. The tubes were slowly heated from 450 °C to 850 °C with a step of 50 °C over a period of 1 week. The initially sintered samples were ground and pressed into round or square-shaped pellets (10 mm diameter, 4 mm thick or $20\times5\times4$ mm^3). The pellets were resealed in evacuated quartz tubes and heated at 950 °C for 3 days. $FeCr_2S_4$ single crystals were grown by the chemical transport reaction method,[12] with chlorine as the transport agent.

Powder x-ray diffraction (XRD) data for polycrystalline samples were collected on a rotating anode x-ray diffractometer, type MXP 18AHF, with graphite monochromatized Cu $K\alpha$ radiation. Single crystal $FeCr_2S_4$ was powdered and diffraction spectrum was taken with the same diffractometer as polycrystals. The orientation of single crystal was determined by the x-ray diffractometer. Room temperature Mössbauer spectra were recorded using a MS-500 Mössbauer spectrometer and ^{57}Co(Pd) radiation source. The measurement of x-ray photoemission spectroscopy (XPS) was carried out on a XPS spectrometer, type VG ESCALAB MKII, with dual-anode x-ray source. The magnetization (M) in the temperature range of 4.2–300 K was measured using an M-9300 vibrating sample magnetometer (VSM). The electron-spin-resonance (ESR) spectra of polycrystalline samples were recorded on the powder samples in a Brucker ER200D spectrometer at 9.61 GHz. The ESR spectra of the single crystal at different directions were collected by the same instrument as polycrystalline samples using polished disks with (111) plane orientation by rotating the slice in a $(1\bar{1}0)$ plane. The slice is perpendicularity to the $(1\bar{1}0)$ plane. (In fact, the different directions are obtained by rotating the magnet.) The measurements of resistance were performed using a standard four-probe method in the temperature range from 4.2 to 300 K.

III. RESULTS AND DISCUSSION

Because In ions are usually in the form of In^{3+} in the compounds, one can image that the heterovalence should be

 ©2005 The American Physical Society

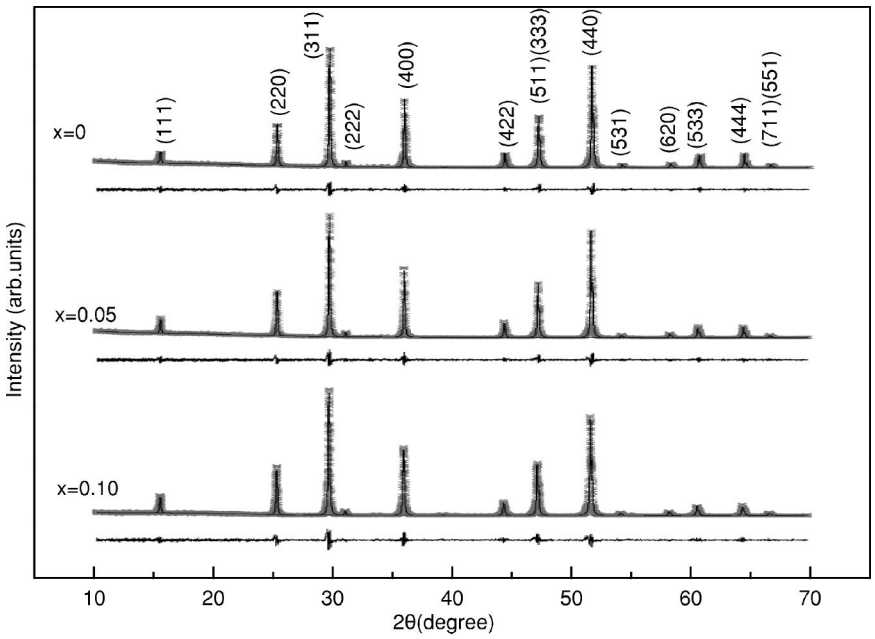

FIG. 1. Powder XRD patterns for $Fe_{1-x}In_xCr_2S_4$ ($x=0,0.05,0.1$) polycrystalline samples.

introduced in the system by the substitution of In for Fe. Thus the system became $Fe^{2+}_{1-2x}Fe^{+}_{x}In^{3+}_{x}Cr^{3+}_{2}S^{2-}_{4}$ or $Fe^{2+}_{1-x}In^{3+}_{x}Cr^{2+}_{2-x}Cr^{3+}_{x}S^{2-}_{4}$. The system can be a CMR material with mixed valence. As is known, the conductive mechanism in the manganites is believed to be the result of DE effect which originated from heterovalence. The initial purpose of this work is to try to introduce the heterovalence in this system by the means of substituting In for Fe, through which the conductive mechanism will be investigated. But the experiments give totally different results.

A. Structure

Figure 1 shows powder XRD patterns of the polycrystalline samples $Fe_{1-x}In_xCr_2S_4$ ($x=0,0.05,0.10$), which exhibit the pure spinel phase. The powder XRD pattern of the single crystal $FeCr_2S_4$ is the same as that of the polycrystal and confirms the pure spinel phase. The crystal structure of polycrystals at room temperature are determined by Rietveld method.[13] It is found that the crystals belong to a normal structure of the cubic system. The space group is F$d3m$. From Fig. 1, one can find a small, systematic change with doping level. By substituting Fe with In, the intensity of (111) increases. The ratio of intensity, for example, I(220)/I(311), also changes. These changes can be attributed to the variation of the structure factor, because the scattering factor of In is different from that of Fe atom. The lattice parameters are listed in Table I. Fe and In atoms occupy the sites 8a $(1/8,1/8,1/8)$. Cr and S atoms occupy the sites 16d $(1/2,1/2,1/2)$, and 32e, respectively. The final R_b factor is 0.0537, 0.0626, and 0.0573, for x=0, 0.5 and 0.10, respectively. These data reveal that In ions are introduced in A sites and there are no replacement between Fe/In atoms and Cr atoms. Upon substitution of Fe by In, no structure change has been observed.

B. Valence and occupancy for Fe, In, and Cr ions

However, it is argued that it is very difficult to rule out some percent of $A-B$ site inversion or a corresponding fraction of In^{3+} due to the resolution of XRD spectra ($\sim 5\%$) despite that the Rietveld analysis proves that Fe and In ions occupy the A sites. To determine the ion distribution and

TABLE I. Lattice parameters, Mössbauer parameters, Curie temperature, T_c^{onset} and T_S for the investigated samples.

	D (Å)[a]	Q_s (mm/s)[b]	I_s (mm/s)[c]	T_c (K)[d]	T_c^{onset} (K)[e]	T_s (K)[f]
$x=0$	9.9941(6)			168	190	130
$x=0.05$	9.9969(8)	0.5395	0	165	178	120
$x=0.1$	10.0072(4)	0.5101	0	161	175	110

[a] D is lattice parameter.
[b] Q_s is quadruple splitting.
[c] I_s is isomer shift.
[d] T_c is Curie temperature.
[e] T_c^{onset} is the temperature below which the magnetization begins to rise.
[f] T_s is the temperature below which ESR spectra split into two lines.

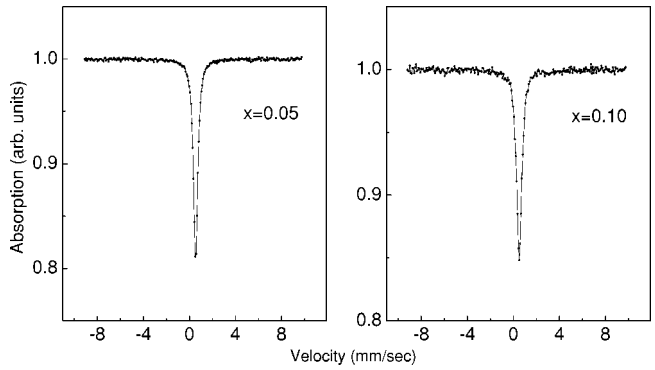

FIG. 2. Mössbauer spectra for $Fe_{1-x}In_xCr_2S_4$ ($x=0.05,0.1$) at room temperature.

valence definitely, Mössbauer and XPS are used to give further information.

In order to determine the valence and occupancy of the Fe ions, Mössbauer measurements were performed at room temperature. The Mössbauer spectra and fitting curves are shown in Fig. 2. Fitting parameters are listed in Table I. As seen from Fig. 2, the spectrum for each sample contains only one absorbing peak with an isomer shift (IS) ~0.5 mm/s and a zero quadruple splitting (QS). These indicate that the Fe ions occupy the tetrahedral sites in the form of Fe^{2+}.[14] Based on the Mössbauer results, we estimate the occupancy of the Fe ions of both doped samples. More than 99% of the Fe ions occupy the *A* sites in the form of Fe^{2+}. Thus, we can conclude that only very little Fe ions reverse to the *B* sites, which can be neglected. Because the samples are solid solution, the Fe and In ions distribute randomly in the *A* sites. Thus, we can plausibly deduce that only little proportion of the In ions which are near to that of the Fe ions reverse to the *B* sites. Such little *A*–*B* site inversion will not affect the properties of the system. Therefore, we can exclude the influence of the *A*–*B* site inversion.

The possibility of mix valence is not excluded completely yet because some percent of Cr atoms may appear in the form of Cr^{2+}. Thus, we perform XPS measurements to determine the valence states of indium and chromium, which are shown in Figs. 3(a) and 3(b). The sharp peaks of Cr $^2p_{2/3}$ and In $^3d_{5/2}$ core levels are located at the position of 575.2 and 444.6 eV, respectively. The sharp peak of In $M_4N_{45}N_{45}$ in the inset of Fig. 3(b) is at 408.2 eV. These results mean that Cr ion is in the form of Cr^{3+} and In ion is in the form of In^{2+}. The peaklike structure around the In $M_4N_{45}N_{45}$ peak located at 408.02 eV has been found to be noise induced. The possibility that a few percent of Cr^{2+} appears in *B* sites then can be ruled out because the same amount of In^{3+} will be induced which will produce another distinct peak in addition to the current observed peak in the XPS spectra of indium. Combined with the XRD analysis, one can reach the conclusion that Cr ion appears in the form of Cr^{3+} and occupies the octahedral site, while In ion is in the In^{2+} valence state and occupies the tetrahedral sites. Thus, the possibility of mixed valence can be ruled out.

C. Magnetism

1. Macromagnetism

The *M*-*H* curves of the $FeCr_2S_4$ at 180 K and 200 K and that of the $Fe_{0.9}In_{0.1}Cr_2S_4$ at 160 K and 180 K are shown in the inset of Figs. 4(b) and 4(d), respectively. The magnetization saturate above ~0.2 T in ferromagneticlike *M*-*H* curve. Therefore, the temperature *T* dependence of the magnetization *M* for $Fe_{1-x}In_xCr_2S_4$ ($x=0,0.05,0.1$) under zero-field cooling (ZFC) and field cooling (FC) in a 0.005 T and 0.5 T magnetic field are shown in Fig. 4, respectively. It can be seen that all the samples undergo a transition from paramagnetic (PM) to ferrimagnetic (FM) phases. In a 0.5 T magnetic field, the magnetization began to raise below a certain temperature T_c^{onset} which is listed in Table I. The *M*-*H* curve display a ferromagneticlike behavior below T_c^{onset} and is paramagnetic above T_c^{onset}. This is a hint that there are no impurity magnetic phase in high temperature in all samples. The obviously irreversibility of curves under ZFC and FC in

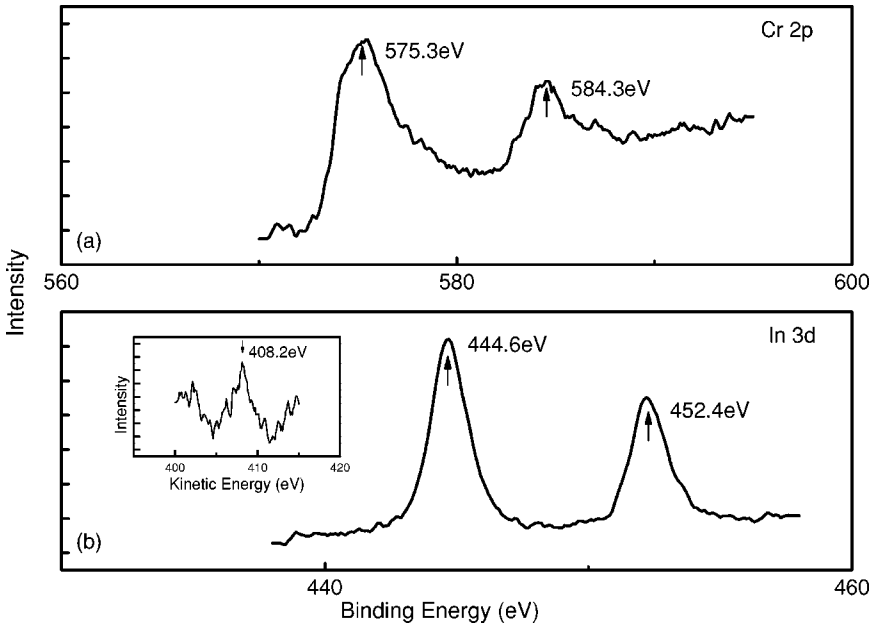

FIG. 3. XPS spectra of (a) Cr 2*p* core level and (b) In 3*d* core level for $Fe_{0.9}In_{0.1}Cr_2S_4$; inset (b) shows the In MNN spectrum.

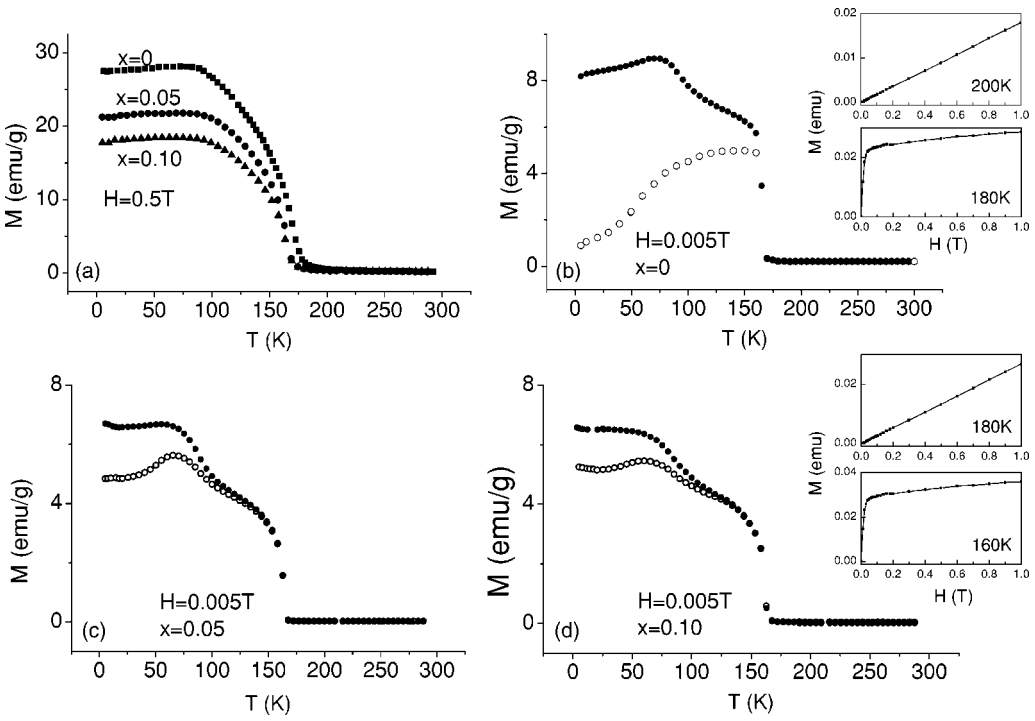

FIG. 4. (a) *M-T* curves for $Fe_{1-x}In_xCr_2S_4$ ($x=0, 0.05, 0.1$) in 0.5 T. (b), (c), (d) show the *M-T* curves under FC (closed circle) and ZFC (open circle) sequences in 0.005 T. The insets in (b) and (d) show the *M-H* curve of $FeCr_2S_4$ and $Fe_{0.9}In_{0.1}Cr_2S_4$, respectively,

0.005 T can be ascribed to magnetic order frustration or a transition into a spin-glass phase.[15,16] In ferrimagnetic material, this can also be attributed to spin reorientation.[17] No irreversibility was observed in applied field of 0.5 T as expected. These results agree with previous reports.[18]

We note that the magnetization M in 0.5 T decreases with increasing x [see Fig. 4(a)]. This is much surprising. The magnetic structure in $FeCr_2S_4$ has been investigated long ago by the powder neutron-diffraction technique, which shows that the spin arrangement in $FeCr_2S_4$ is simple Nèel type with the magnetic moment of Cr ion is in the direction of applied field and the magnetic moment of Fe ion is in the direction opposite to that of the applied field.[19] Then according to Nèel's two-sublattice model, for $FeCr_2S_4$, both the Fe sublattice and Cr sublattice are ferromagnetic, while the magnetic moment of Fe sublattice is antiparallel to that of the Cr sublattice due to the magnetic coupling between two sublattices. Thus, the net magnetization M_s can be written as $M_s=M_{Cr}-M_{Fe}$, where M_{Cr} and M_{Fe} are the spontaneous magnetization of the Cr and Fe sublattices, respectively. In previous studies by doping in Cr sites, M_s does decrease with increasing of doping level because M_{Cr} decreases with increasing x.[18] One can image that in $Fe_{1-x}In_xCr_2S_4$ system, the substitution of nonmagnetic In ions for Fe ions will dilute the Fe sublattice, thus M_{Fe} will decrease with increasing x. It seems that M_s should increase with increasing doping level. But the experimental results prove that M_s decreases with increasing doping level, which imply only that M_{Cr} should decrease.

It is known that there are at least two kinds of Cr-Cr magnetic interactions in ACr_2S_4 compounds, namely the nearest-neighbor ferromagnetic Cr-Cr interaction, and the more distant neighbor antiferromagnetic Cr-Cr interactions. Both the nearest-neighbor ferromagnetic Cr-Cr interaction, and the more distant neighbor antiferromagnetic Cr-Cr interactions are modulated by the distance between Cr ions and in turn by the lattice parameter.[20] The radium of the Fe^{2+} lies between that of Zn^{2+} and that of Cd^{2+}. Comparing the lattice parameter of the $Fe_{1-x}In_xCr_2S_4$ (see Table I) to that of $ZnCr_2S_4$ (9.988 Å) and that of $CdCr_2S_4$ (10.244 Å),[20] the lattice parameters of $Fe_{1-x}In_xCr_2S_4$ are almost identical to that of $ZnCr_2S_4$ but considerably smaller than that of $CdCr_2S_4$. Thus, $ZnCr_2S_4$ should be taken as a reference for the *B-B* interaction of $Fe_{1-x}In_xCr_2S_4$. In $ZnCr_2S_4$, the sum of the nearest-neighbor ferromagnetic Cr-Cr interactions is smaller than the sum of the more distant neighbor antiferromagnetic Cr-Cr interactions, thus the overall Cr-Cr interaction is antiferromagnetic.[20] There is no magnetic coupling between A and B sublattices in $ZnCr_2S_4$. A remarkable feature of $FeCr_2S_4$ spinel is that all exchange integrals J_{AA} (or $J_{Fe\text{-}Fe}$), J_{AB} (or $J_{Fe\text{-}Cr}$) and J_{BB} (or $J_{Cr\text{-}Cr}$) are negative and favor antiparallel alignment of the spins connected by the interaction.[21] But the *AB* (or Fe-Cr) interaction is the strongest, so that the A (or Fe) spins are parallel to each other and the B (or Cr) spins are parallel to each other, just in order that the A (or Fe) spins may be antiparallel to the B (or Cr) spins. The magnetism of Fe sublattice is reduced due to the dilution of the Fe sublattice by the nonmagnetic In ions in $Fe_{1-x}In_xCr_2S_4$. The magnetic coupling between two sublattices is weakened subsequently and thus spins in Cr sublattice will not align parallel perfectly as before and prefer to align antiparallel. Hence M_{Cr} decreases with increasing doping level. The net magnetization will decrease as a result.

As is known, Curie temperature T_c, obtained by the inflection point of $M(T)$, is determined by all exchange inter-

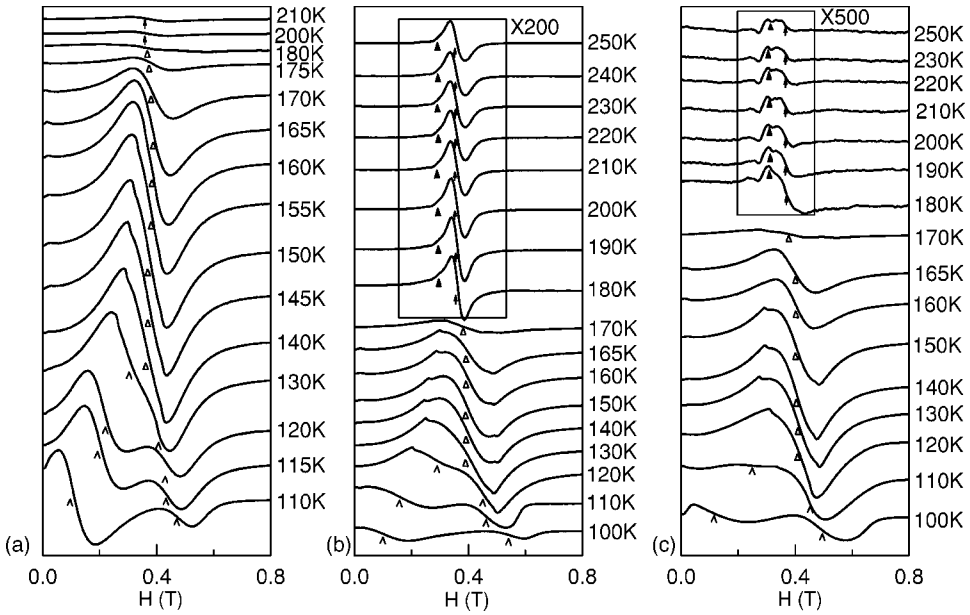

FIG. 5. ESR spectra of $Fe_{1-x}In_xCr_2S_4$ at different temperature. (a) $x=0$, (b) $x=0.05$, (c) $x=0.1$. Dark arrows "↑" mark the single PM line above T_c^{onset}, "∧" marks the splitting peaks. The peaks marked by the open triangle "△" is attributed to the ferrimagnetic nature of the system. Anomalies marked by the closed triangle "▲" are due to the magnetic fluctuation embedded in the paramagnetic matrix (see text). The spectra in the insets have been enlarged by a factor of 200 and 500 for $x=0.05$ and 0.10, respectively.

actions. The doping suppress these exchange interactions. Therefore, T_c decreases with increasing doping level (shown in Table I).

2. Micromagnetism

Obviously, the magnetism should also reflect in micromagnetism of the system. Here we further investigated the micromagnetism by the ESR. Figure 5 shows the ESR spectra for the polycrystalline samples with $x=0,0.05,0.10$ at different temperature.

For the undoped sample, the ESR spectra consist of a single line with $g\sim 2.0$ which is marked by "↑" above T_c^{onset}. This signal has been believed to be originated from the PM state in both Cr and Fe sublattice layers. But in doped sample, there are some anomaly peaks which are marked by "▲" except for the PM line with $g\sim 2.0$ above T_c. These anomaly peaks became more obvious in higher doping level. Because we have excluded the possibility of the existence of the impurity phase, such anomalies can be attributed to the magnetic fluctuation embedded in the paramagnetic matrix. But because there are large anisotropy in the $FeCr_2S_4$ series, the anisotropy of the g factor may contribute to such anomalies in polycrystal too.

Below T_c^{onset}, there is only a single line with $g<2$ which is marked by "△." This is attributed to the ferrimagnetism nature of the system. As temperature decreases below T_s (defined as the temperature below which ESR spectra split into two lines), the ESR line splits into two lines which is marked by "∧," shifting to higher and lower fields with decreasing temperature, respectively. T_s decrease with increasing doping level (see Table I). This is a hint of the lowering of anisotropy with increasing doping level.

The ESR behavior in $FeCr_2S_4$ system is obviously different from that of manganites. Generally, in the manganites, ESR line with $g>2$ or coexistence of ESR lines with $g\sim 2$ and $g>2$ should appear below T_c. And the ESR line with $g>2$ will shift to lower field with decreasing temperature.[22] The ESR line with $g>2$ is generally attributed to the FM state at $T<T_c$.

Turskan *et al.* present the angular dependence of the resonance field of ESR spectra for the $FeCr_2S_4$ single crystal with (110) plane orientation and the intensity of ESR spectra along three principle crystal axes.[23] The results clearly show that ESR spectrum depend on the orientation drastically. We suggest that the polycrystalline samples can be treated as a collection of many small single crystals with different crystal orientation. Thus, the ESR spectra of the polycrystalline samples should be the overlapping of the ESR spectra of the single crystal with different magnetic field orientation. But as the intensity is given only along three principle crystal axes in a previous report,[23] the overlapping of different angles cannot be obtained directly. In order to understand the extraordinary ESR spectra of $FeCr_2S_4$ polycrystal, we perform the ESR study on $FeCr_2S_4$ single crystal from 0° to 180° at an interval of 10° by rotating the sample in plane $(1\bar{1}0)$ at 170 K and 110 K, respectively. The reason to choose 170 K and 110 K is that 170 K is the typical temperature of a single ESR line in the PM state and 110 K is the typical temperature of two splitting ESR lines in the FM state. In Figs. 6(a) and 6(b), we display the results of the ESR lines as a function of angle $\theta(0°-180°)$ at an interval of 10° at 170 K and 110 K, respectively. At 170 K, the ESR lines translate from $H_{res}\sim 0.396$ T to $H_{res}\sim 0.421$ T from 0° to 90° gradually. The ESR lines from 100° to 180° is just the reverse. For 110 K, however, the experiments give very complex image. From 0° to 90°, the ESR lines can be divided into two groups which are located near $H_{res}\sim 0.24$ T and $H_{res}\sim 0.576$ T, respectively. The resonance field of the ESR lines from 100° to 180° transit from 0.35 T to 0.52 T gradually. And the intensity of the ESR line with different angle is different. We display the overlapping of all ESR lines with different angles at 170 K and 110 K in Figs. 6(c) and 6(d), respectively. One can find that the overlapped spectrum at 170 K consist of a single ESR line with $H_{res}\sim 0.41$ T at 170 K [see Fig. 6(c)] and the overlapped spectrum consist of two ESR lines with

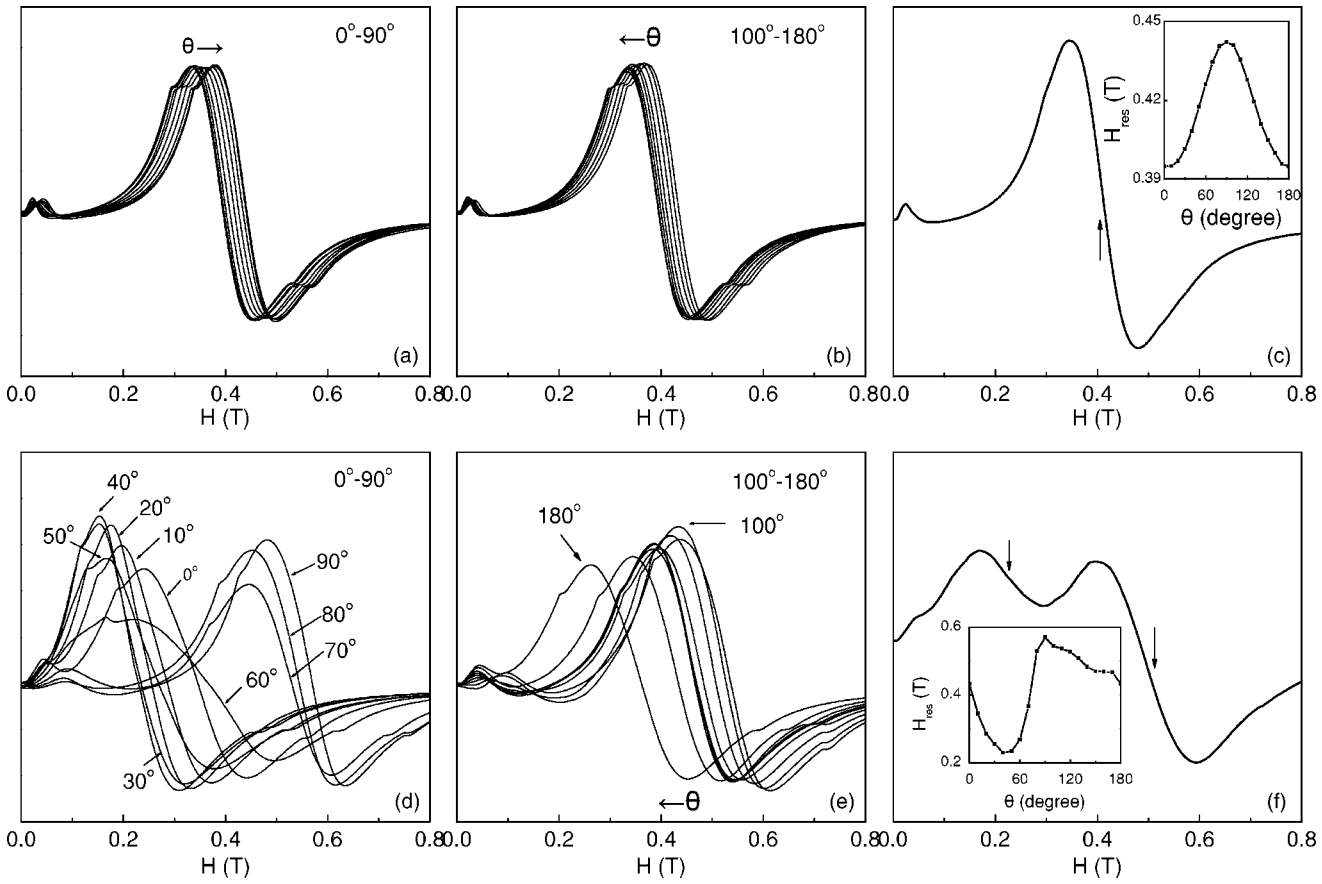

FIG. 6. The ESR line of the $FeCr_2S_4$ single crystal as a function of angle $\theta(0°-180°)$ at an interval of 10° at (a) 170 K and (b) 110 K, respectively. The overlapping of all ESR lines with different angle is shown in (c) and (d), respectively. Insets in (c) and (d) show the relation between resonance field H_{res} and angle θ.

$H_{res}\sim 0.23$ T and $H_{res}\sim 0.5$ T at 110 K [see Fig. 6(d)]. The results of the overlapped spectra obtained by overlapping over a plane coincide with the experiments qualitatively [see the ESR line at 170 K and 110 K in Fig. 5(a)], although a quantitative explanation require overlapping over the full space. These results show that the splitting ESR spectra of $FeCr_2S_4$ polycrystal is due to the large anisotropy.

Now we turn to the question of what is the origin of the anomalies in ESR lines. First we consider the possibility that the anomalies of ESR signal come from the anisotropy of the *g* factor and/or the polycrystalline nature of the samples. To elucidate this question, measurements in the single crystal will be helpful. The splitting of the ESR spectra is attributed to the large anisotropy according to the above discussion. From Fig. 5 we can conclude that there are large anisotropy in all samples. Therefore, both undoped and doped samples will suffer the influence of the anisotropy inevitably. Thus, the anomalies should also appear in the ESR signal of the undoped sample. In Fig. 7 we present the ESR spectra of the undoped polycrystalline samples at 200 K and that of the undoped single crystal samples at 180 K and 200 K. No such anomalies observed in the ESR spectra of the doped samples appear. In fact, the anisotropy of the $FeCr_2S_4$ series is very low in the PM region, as shown in Fig. 6(a). Thus, we can conclude that the anomalies of the ESR signal do not originate from the anisotropy of the *g* factor and/or the polycrys-

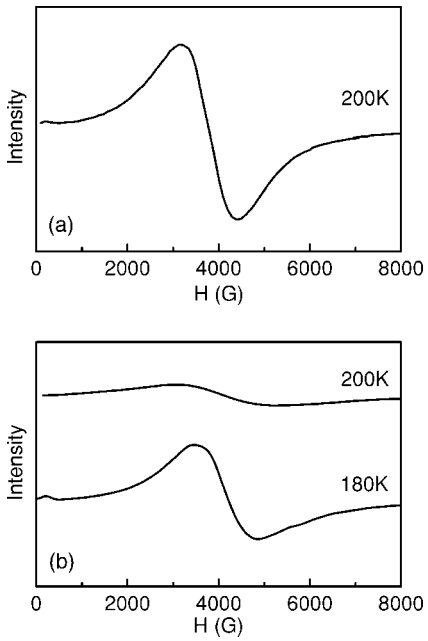

FIG. 7. (a) The ESR signal of the $FeCr_2S_4$ polycrystal at 200 K. (b) The ESR signal of the $FeCr_2S_4$ single crystal at 180 K and 200 K.

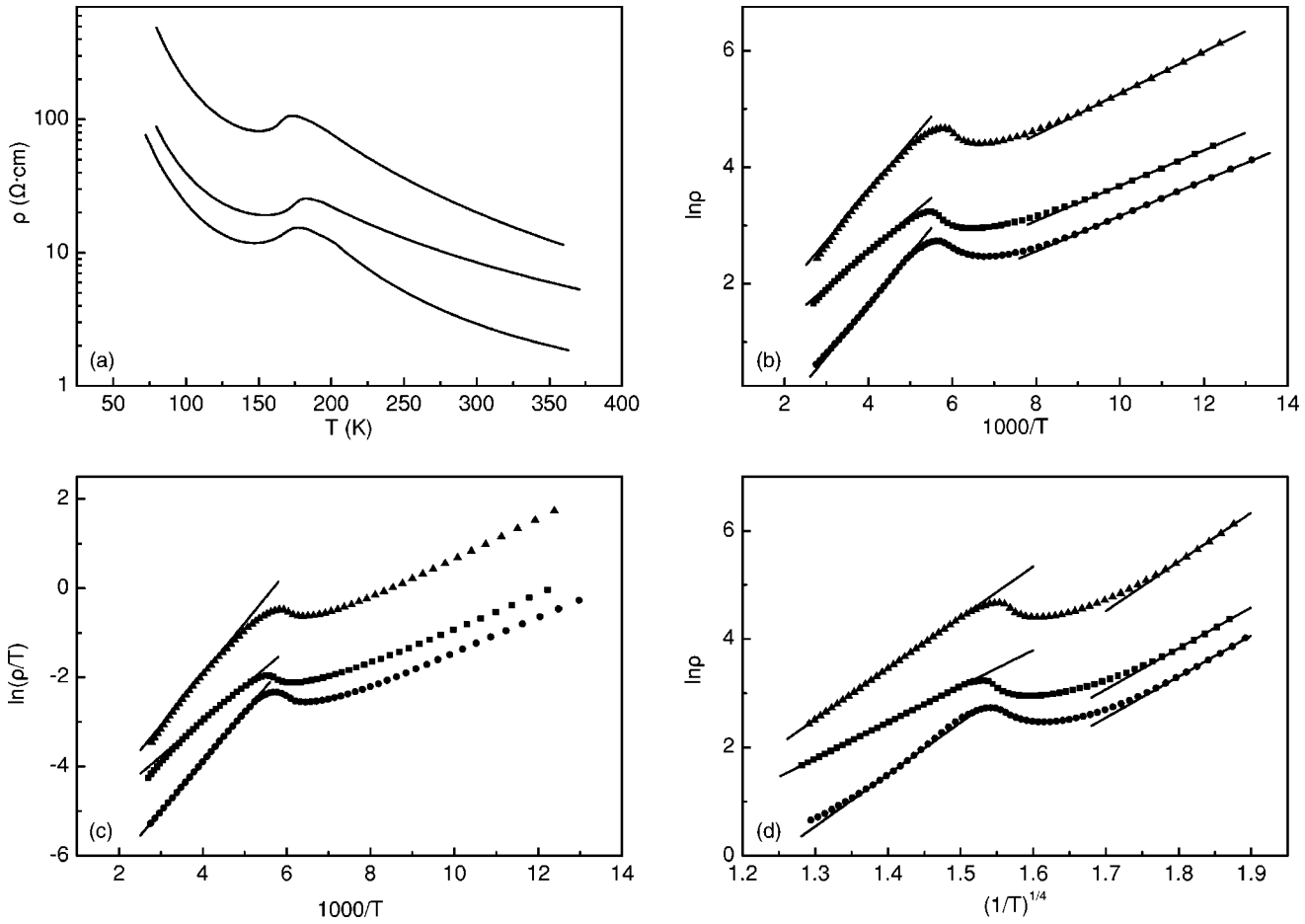

FIG. 8. (a) The temperature dependence of resistivity ρ in zero magnetic field for $Fe_{1-x}In_xCr_2S_4$ ($x=0, 0.05, 0.1$). (b),(c),(d) Zero-field resistivity curves for $Fe_{1-x}In_xCr_2S_4$ ($x=0.05, 0.1$) replotted as $\ln\rho \sim 1000/T$ (closed circle), $\ln(\rho/T \sim 1000/T)$ (solid square), $\ln\rho \sim (1000/T)^{1/4}$ (solid triangle), respectively. The solid lines are the linear fitting curves.

talline nature of the sample. Therefore, the anomalies should be ascribed to the magnetic fluctuation embedded in the paramagnetic matrix. We further evaluate the origin of the magnetic fluctuation. Because the radium of the nonmagnetic In ion is much larger than that of the Fe ion, the existence of the In ions will block the correlation between the Fe ions which are closed to the In ions. Thus, the magnetic fluctuation will appear in the paramagnetic matrix.

D. VRH mechanism above T_c

As magnetism and transport property is closely related in chalcogenide spinels, the magnetism will inevitably affect the transport property. The temperature dependence of resistance in zero magnetic field for doped samples is shown in Fig. 8(a). The curves show obviously that the resistivity increases with increasing doping level. The resistance in zero field increases rapidly with decreasing temperature, and reaches a maximum around T_c. As the temperature is further reduced, ρ falls abruptly in the narrow temperature region and then increases again below T_m (defined as the temperature corresponding to the minimum resistivity below T_c, shown in Table II). Both above T_c and below T_m, semiconductorlike transport behavior is observed. As is known, for semiconductorlike transport behavior, there are three models. (1) An Arrhenius law, $\rho=\rho_0 \exp(E/k_BT)$, is generally used to model activated behavior due to a band gap E or mobility edge. (2) Nearest-neighbor hopping of small polarons, $\rho=\rho_0 T \exp(E_p/k_BT)$. (3) If the carriers are localized by random potential, Mott's VRH expression $\rho=\rho_0 \exp(T_0/T)^{1/4}$ is appropriate.[24–26] Thus, in order to understand the transport mechanism in this system, it is necessary to fit the resistivity curves both above T_c and below T_m based on these three descriptions.

In Figs. 8(b)–8(d), the zero-field $\rho(T)$ curves are replotted as $\ln\rho \sim (1000/T)$, $\ln(\rho/T) \sim (1000/T)$, $\ln\rho \sim (1000/T)^{1/4}$, respectively. The solid lines are a fit for a different model. The fitted parameters are listed in Table II. For $FeCr_2S_4$, the fit of the small polaron hopping model remarkably agrees with the data in the temperature range above ~192 K. Although the other two models agree with the data in some limited temperature above T_c, deviations can be seen at higher temperatures. Thus, the data of $FeCr_2S_4$ is clearly in favor of the small polaron hopping model in the high temperature range. In the temperature below T_c, the fit of the VRH model agrees with the data below ~84 K. The fit of the thermal activation model agrees with the data in a much broader temperature (below ~112 K). The data are clearly in

TABLE II. Fitting parameters of the various samples for the thermal activation, the small polaron hopping and the variable-range hopping (VRH) model. The values in parentheses are the temperature above which only a limited regime can be fitted by the model.

	T^{above} (K)			T^{down} (K)		
	$\ln\rho\sim 1000/T$	$\ln(\rho/T)\sim 1000/T$	VRH[a]	$\ln\rho\sim 1000/T$	VRH[b]	T_m[c]
$x=0$	(197)	192	(214)	112	84	156
$x=0.05$	(202)	(197)	190	103	91	154
$x=0.1$	(210)	(208)	187	105	98	150

[a]T^{above} is the lowest temperature deviated from linear in the high temperature region.
[b]T^{down} is the highest temperature deviated from linear in the low temperature region.
[c]T_m is the temperature corresponding to the minimum resistivity below T_c.

favor of the thermal activation model in the low temperature range. These results of undoped samples are consistent with previous reports.[11] For doped samples, the resistivity can be fitted to the small polaron hopping model and/or thermal activation model in a limited temperature range; deviations, however, are seen at higher temperature. The VRH model gives a convincing fit above the Curie temperature. In the low temperature, however, the thermal activation model fit the resistivity below $\sim$105 K for both samples. The VRH model agrees with the data in a narrower temperature range. These results are in favor of the thermal activation model in the low temperature range. As is known, the VRH model dominates the transport behavior when there are random potential. In our doped samples, the magnetic fluctuation is found in the high temperature regime. The magnetic random potential will appear and trap the carrier. Also, the hopping across the grain boundaries is the variable-range case and will contribute to the whole transport process at high temperature. Because the magnetic fluctuation disappears in the low temperature regime and the possibility of the hopping across the grain boundaries decreases drastically at low temperature, thermal activation dominates the transport behavior. Thus, the transport behavior in doped samples can be well understood.

IV. CONCLUSION

In conclusion, the magnetic and transport properties of $Fe_{1-x}In_xCr_2S_4$ ($x=0, 0.05, 0.10$) are studied. The experimental results of ESR indicate clearly that there is the magnetic fluctuation above T_c in doped samples. The random magnetic potential is induced and resulted in the localization of the carriers. Thus the VRH mechanism dominates the transport properties above T_c in the doped sample. We suggest that the polycrystal can be treated as a collection of many small crystals with different orientation. Thus, the ESR spectra of the polycrystal should be the overlapping of the ESR spectra of the single crystal with different magnetic field orientation. By studying the ESR lines of the single crystal with different angle, we explain the unusual ESR behavior appropriately, i.e., there is only a single line with $g<2$ below T_c^{onset} while there are two splitting peaks below T_s in polycrystal.

ACKNOWLEDGMENTS

This work was supported by the National Science Foundation of China under Grant No. 10334090 and the State Key Project of Fundamental Research, China (Grant No. 001CB610604).

*Electronic address: zhangyh@ustc.edu.cn

[1] J. M. D. Coey, M. Viret, and S. von Molnar, Adv. Phys. **48**, 167 (1999).
[2] *Colossal Magnetoresistive Oxides*, edited by Y. Tokura (Gordon and Breach, Amsterdam, 2000).
[3] E. L. Nagaev, Phys. Rep. **346**, 387 (2001).
[4] M. B. Salamon and M. Jaime, Rev. Mod. Phys. **73**, 583 (2001).
[5] C. Zener, Phys. Rev. **82**, 403 (1951).
[6] A. J. Millis, P. B. Littlewood, and B. I. Shraiman, Phys. Rev. Lett. **74**, 5144 (1995).
[7] A. P. Ramirez, R. J. Cava, and J. Krajewski, Nature (London) **386**, 156 (1997).
[8] Z. W. Chen, S. Tan, Z. R. Yang, and Y. H. Zhang, Phys. Rev. B **59**, 11172 (1999).
[9] J. B. Goodenough, J. Phys. Chem. Solids **30**, 261 (1969).
[10] P. F. Bongers, C. Haas, A. M. J. G. Van Run, and G. Zanmarchi, J. Appl. Phys. **40**, 958 (1969).
[11] Z. R. Yang, S. Tan, Z. W. Chen, and Y. H. Zhang, Phys. Rev. B **62**, 13872 (2000).
[12] T. Watanable, J. Phys. Soc. Jpn. **32**, 1443 (1972).
[13] H. M. Rietveld, J. Appl. Crystallogr. **2**, 65 (1969).
[14] E. Riedel and R. Karl, J. Solid State Chem. **38**, 40 (1981).
[15] K. Binder and A. P. Young, Rev. Mod. Phys. **58**, 801 (1986).
[16] X. X. Zhang, R. H. Yu, J. Tejada, G. G. Sun, Y. Xin, and K. W. Wong, Appl. Phys. Lett. **68**, 22 (1996).
[17] G. Srinivasan and Mohindar S. Seehra, Phys. Rev. B **28**, 1 (1983).
[18] Z. Yang, S. Tan, and Y. H. Zhang, Phys. Rev. B **64**, 024401 (2001); Z. Yang, S. Tan, and Y. H. Zhang, *ibid.* **65**, 184404 (2002).
[19] G. Shirane, D. E. Cox, and S. J. Pickart, J. Appl. Phys. **35**, 954 (1964).

[20] P. K. Baltzer, P. J. Wojtowicz, M. Robbins, and E. Lopatin, Phys. Rev. **151**, 357 (1966).
[21] *Introduction to Solid State Physics*, 6th ed., edited by C. Kittel, (Wiley, New York, 1986).
[22] X. M. Liu, X. J. Xu, and Y. H. Zhang, Phys. Rev. B **62**, 15112 (2000).
[23] V. Tsurkan, M. Lohmann, H.-A. Krug von Nidda, A. Loidl, S. Horn, and R. Tidecks, Phys. Rev. B **63**, 125209 (2001).
[24] R. M. Kusters, J. Singleton, D. A. Keen, R. McGreevy, and W. Hayes, Physica B **155**, 362 (1989).
[25] M. Viret, L. Ranno, and J. M. D. Coey, Phys. Rev. B **55**, 8067 (1997).
[26] G. J. Snyder, R. Hiskes, S. DiCarolis, M. R. Beasley, and T. H. Geballe, Phys. Rev. B **53**, 14434 (1996).